J Appl Electrochem (2009) 39:45–53
DOI 10.1007/s10800-008-9638-8

ORIGINAL PAPER

Methanol tolerant oxygen-reduction activity of carbon supported platinum–bismuth bimetallic nanoparticles

C. Jeyabharathi · J. Mathiyarasu · K. L. N. Phani

Received: 3 April 2008 / Accepted: 7 July 2008 / Published online: 25 July 2008

Abstract The oxygen reduction activity and methanol tolerance of Pt–Bi/C electrocatalysts were studied using electrochemical voltammetric techniques including rotating ring-disk electrode. The Pt–Bi/C catalyst was prepared via a polyol method and subjected to heat treatment to increase the degree of alloying. X-ray diffraction studies revealed the unalloyed character of the as-prepared catalyst and alloy formation upon heat treatment. The electrochemical behaviour of both catalysts showed different behaviour in dilute acid electrolytes, namely sulphuric and perchloric acids. In both electrolytes, the oxygen reduction reaction was found to occur via the four-electron process revealing that the mechanism of oxygen reduction is unaltered even in the presence of excess of methanol. Pt–Bi/C catalyst material showed dramatically different properties and reactivity with respect to oxygen reduction activity and methanol tolerance in perchloric and sulphuric acids. The onset potential for oxygen reduction reaction (ORR) significantly shifted by about 100 mV to more negative values and at the same time the current density was significantly enhanced. This type of non-ideal methanol-tolerant behaviour among Pt bimetallics and a "trade off" is common with all the known so-called methanol tolerant combinations of Pt. In general, the Pt–Bi surface appeared to have a negligibly lesser sensitivity towards methanol activity compared to pure platinum.

Keywords Electro catalysis · Methanol tolerant · Acid electrolyte · Platinum–bismuth · Rotating ring disk · Oxygen reduction

C. Jeyabharathi · J. Mathiyarasu (✉) · K. L. N. Phani
Electrodics and Electrocatalysis Division,
Central Electrochemical Research Institute,
Karaikudi 630006, India
e-mail: al_mathi@yahoo.com

1 Introduction

Though alcohol based fuel cells have reached the commercial stage, there is still continued developmental activity because of the high permeation of methanol through the membrane, which is known as methanol cross-over, in turn affecting the cathode catalyst activity [1]. This cross-over problem has been addressed by (i) increasing the membrane thickness; (ii) modifying the membrane with a hybrid/composite material and (iii) by decreasing the methanol concentration in the anolyte compartment. Apart from these, the development of cathode materials that are immune to methanol may constitute a novel approach to deal with this cross-over problem.

Several investigations for the development of methanol tolerant cathode catalysts replacing the present best cathode catalyst platinum-carbon are underway. They are namely, (i) metallo-porphyrins/phthalocyanine complexes [2–5], (ii) chalcogenides/chevrel based catalyst [6–9] (iii) non-noble metal such as palladium [10–17] and (iv) binary platinum alloys where the secondary elements are Ni, Cr, Co, Fe, Bi [18–30].

Continuous efforts are being invested in synthesizing alloy nanoparticles, for example of Pt and Pd by addition of a secondary metal element in order to design surfaces with increased catalytic activity as compared to that of the pure metal particle. Initially, the Pt–Bi bimetallic alloy catalyst was established as an anode catalyst for formic acid oxidation where it showed excellent poison-removing effects and it is widely used as direct formic acid fuel cell (DFFC) anode catalyst material [29, 31–38]. Pt–Bi catalysts when used in acidic environment lack stability. It has been reported that the stability of the fuel cell catalyst material can be enhanced by heat treatment at a desired temperature. In general, the heat treatment of the binary metal catalyst

favours the degree of alloying, removes the residual organics adsorbed on the electrocatalysts and improves the overall catalyst performance [39].

Pt–Bi is found to be superior for formic acid oxidation than methanol oxidation and further it is reported that it is immune to methanol oxidation [29, 31]. Inhibition of methanol oxidation at bismuth-modified Pt(100) electrodes was earlier explained by Campbell and Parsons [31] that the platinum sites vacated by bismuth desorption are amenable to blocking by the poison produced during methanol oxidation. However, the reports thus far published have hardly revealed the mechanism behind the so-called methanol tolerance of Pt–Bi. Recently, Pt–Bi has been reported as a methanol tolerant cathode catalyst material [28]. However, the paper lacks necessary data to establish conclusively the ORR activity and the factors that influence the methanol tolerance character of the catalyst. The observations and interpretation appear to be based on incomplete studies that needed [40, 41] thorough analysis before deciding if the catalysts are methanol tolerant and ORR active. It is also noted that details of the oxygen reduction reaction and the possible role of bismuth have not been studied so far. It appears certain that the dissolution of the secondary metal/non-metal occurs in the oxidation or reduction reactions on Pt–Bi. Based on our own experience and the available literature information, we realize the possible role played by the acid electrolyte employed in characterizing Pt–Bi catalysts.

Methanol tolerance and ORR activity of the Pt–Bi catalyst strongly depend on the acid electrolyte used in the cell, sulphate versus perchlorate. We synthesize carbon-supported platinum–bismuth bimetallic nanoparticles by polyol synthesis and investigate its ORR activity in sulphuric and perchloric acid electrolytes in the presence and absence of methanol, using hydrodynamic voltammetry and a ring-disk electrode.

2 Experimental

2.1 Materials

All chemicals used were of analytical grade. $H_2PtCl_6 \cdot 6H_2O$, GR (Merck) and $Bi(NO_3)_3 \cdot 5H_2O$, GR (Merck) were used as metal precursors. Vulcan-XC72R (Cabot Corporation, USA) was used for supporting the metal nanoparticles. Ethylene glycol, GR (Merck) was used as a solvent and reducing agent. All the solutions were prepared with ultra-pure water (MilliQ, Millipore).

2.2 Synthesis of metal nanoparticle catalyst

Pt–Bi (70:30)/C nanoparticles were prepared by adopting a polyol process of the type reported elsewhere [42]. In this procedure, 9.28 mg of $H_2PtCl_6 \cdot 6H_2O$, 34.8 mg of $Bi(NO_3)_3 \cdot 5H_2O$ and 125 mg of Vulcan-XC72R carbon were taken in a 100 mL round bottom flask. To this 40 mL of ethylene glycol was added and stirred well to get a homogeneous mixture. This mixture was refluxed at ca. 85 °C for 4 h in a heating mantle. The mixture was kept aside to cool at room temperature. After cooling, the black powders were centrifuged and washed three times with Millipore water (18.2 MΩ cm^{-1}) and with acetone. Then the powders were kept in a vacuum oven for drying at room temperature. The synthesized metal nanoparticles were subjected to heat treatment in argon atmosphere at 500 °C for 3 h in a tubular furnace.

2.3 X-ray diffraction

X-ray diffraction (XRD) measurements of Pt–Bi carbon-supported catalysts were carried out on a Philips PANanalytical X-ray diffractometer using CuK_α radiation ($\lambda = 0.15406$ nm). The XRD patterns were obtained using high resolution in the step-scanning mode with a narrow slit (0.5°) with a counting time of 15 s per 0.1°. Scans were recorded in the 2θ range of 15–90°. The identification of the phases was made by referring to the Joint Committee on Powder diffraction Standards International Center for Diffraction Data (JCPDS-ICDD) database. Pt/C (20 wt%) (E-Tek) sample was purchased from E-Tek Division of De Nora N.A., Inc.

2.4 Transmission electron microscopy

Transmission electron microscopic (TEM) analysis was carried out using a JEOL-JEM-3010-URP microscope operating at 300 kV and having a resolution of 0.17 nm. The samples for the TEM characterization were prepared as follows: a carbon film was deposited onto a mica sheet that was placed onto the Cu grids (300 mesh and 3 mm diameter). The material to be examined was dispersed in water by sonication, placed onto the carbon film and left to dry. The average particle size was calculated using about 300 particles.

2.5 Electrochemical analysis

The performance of Pt–Bi/C alloy catalysts and a commercial Pt/C (20 wt%, E-Tek) catalyst for the ORR was evaluated preliminarily with a half-cell configuration based on the linear scan voltammetric (LSV) measurements. Ten milligrams of catalysts, 0.5 mL of Nafion solution (5 wt%, Aldrich) and 2.5 mL of water were mixed ultrasonically. A measured volume (3 or 10 μL) of this ink was transferred via a syringe onto a freshly polished glassy carbon disk (3 or 6 mm in diameter). After the solvents were evaporated

overnight at room temperature, the prepared electrode served as the working electrode.

Electrochemical measurements were performed using a BAS 100B or Autolab PGSTAT 30 potentiostat/galvanostat (for RRDE experiments where the equipment is coupled with a BIPOT module) and a conventional three-electrode electrochemical cell. The counter electrode was a platinum foil and a mercury/mercurous sulphate electrode and calomel electrode served as the reference electrode. However, all potentials are referred to the Ag/AgCl. The electrolyte used for half-cell measurements was 0.5 M H_2SO_4 or 0.1 M $HClO_4$ + 0.5 M CH_3OH. Due to a slight contamination from the Nafion solution, the porous electrodes were cycled at 50 mV s^{-1} between −200 and 700 mV versus Ag/AgCl until reproducible cyclic voltammograms were obtained, prior to any LSV measurements. The electrochemical activity for the ORR was measured with the rotating ring disk electrode (RRDE) technique using an interchangeable ring-disk electrode setup coupled with a rotation controller (Pine Instruments). High purity nitrogen and oxygen were used for de-aeration and aeration of the solutions, respectively. During the measurements, a blanket of nitrogen or oxygen was maintained above the electrolyte surface. Unless stated otherwise, all half-cell tests were performed at a temperature of 25 ± 1 °C.

3 Results and discussion

3.1 Physical characterization of nanoparticulate Pt–Bi/C

Figure 1a shows the XRD patterns of the as-prepared carbon supported Pt–Bi nanoparticles. The peaks appearing at 40.09, 46.67, 67.63, 81.83 and 85.82 corresponds to the 111, 200, 220, 311 and 222 phases of the platinum *fcc* crystal system. The broad peak observed at ∼25° corresponds to the vulcan carbon peak which was observed by several authors [14, 18]. Peak broadening suggests smaller particle size. The other reflections with smaller intensity can be indexed to BiO, Bi_2O_3, etc. The particle size of the Pt–Bi calculated based on the Scherrer equation was found to be ∼24 nm which was further confirmed by the TEM measurements (Fig. 1a inset), that show an average particle size of ∼20 ± 2 nm. Thus, the Pt–Bi nanoparticles supported on carbon appear to be a simple solid solution of platinum and bismuth oxides. Figure 1b shows the XRD patterns of the Pt–Bi/C catalyst which is heat treated at 500 °C in argon atmosphere for 3 h. When compared to the as-prepared catalyst sample, a shift in the 2θ values corresponding to the platinum phases was observed suggesting a change in the crystal lattice size. The platinum lattice size is 0.3923 nm (JCPDS Card 00-005-0681), whereas the as-prepared Pt–Bi/C shows a lattice parameter of 0.3914 nm

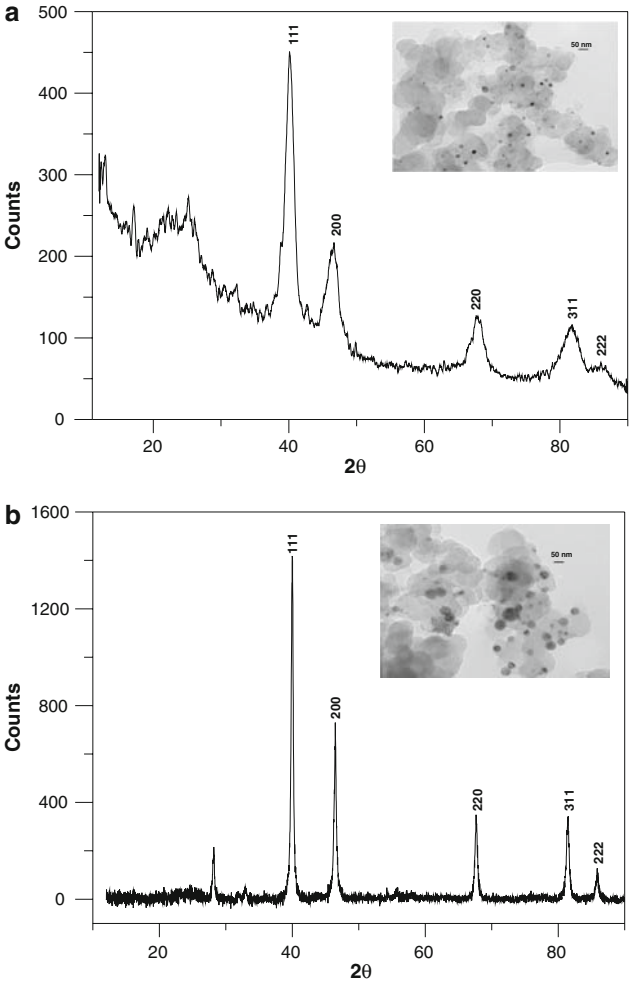

Fig. 1 XRD patterns of Pt–Bi/C (**a**) as-prepared & (**b**) heat treated

and on heat treatment, a shrink in the crystal lattice size (ca. 0.3904) was observed. According to Rivera et al. [35], this can be attributed to the incorporation of Bi within the platinum crystal lattices which leads to the Pt–Bi alloy formation and this alters the Pt–Pt bond distance. When compared to the untreated one, the XRD pattern of heat treated Pt–Bi does not show any Bi or BiO peak in addition to the Pt peaks. The intensity and sharpness of reflections suggest that the alloy particles formed upon heat treatment, agglomerate leading to an increase in the particle size. Thus, heat treatment results in the sintering of the nanoparticles, causing an increase in the particle size and reduction in the surface area [33]. The particle size calculated based on Scherrer equation was found to be ∼40 nm.

3.2 Electrochemical characterization of nanoparticulate Pt–Bi

Figure 2 shows the cyclic voltammogram of Pt–Bi/C obtained in 0.5 M sulphuric acid at 100 mV s^{-1} over the

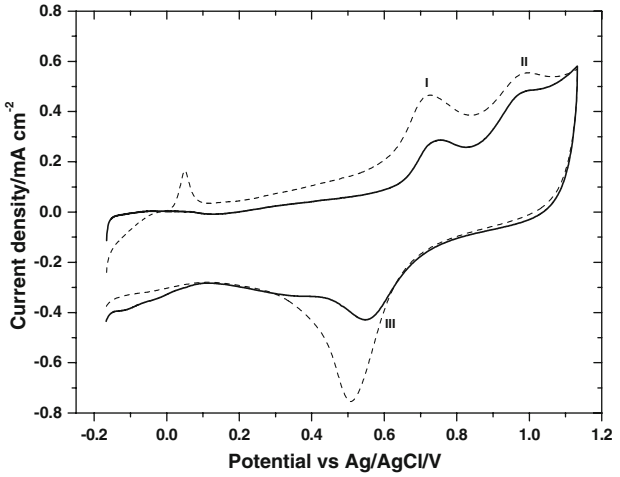

Fig. 2 Cyclic voltammograms of as-prepared (*dotted line*) and heat-treated (*solid line*) Pt–Bi/C catalysts in 0.5 M sulphuric acid

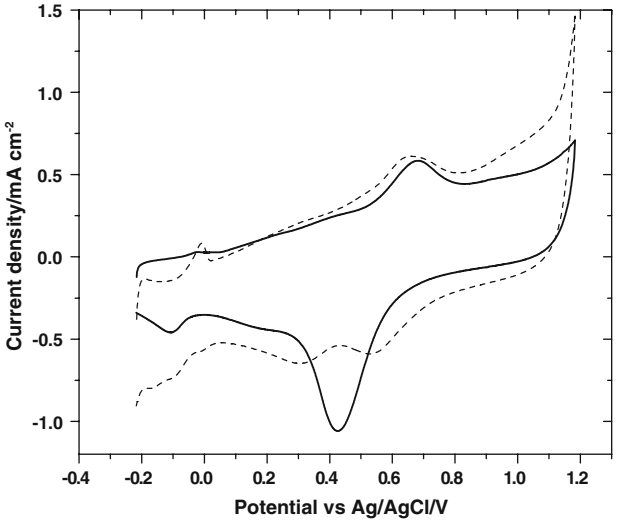

Fig. 3 Cyclic voltammograms of as-prepared (*dotted line*) and heat-treated (*solid line*) Pt–Bi/C catalysts in 0.1 M perchloric acid

potential range from −200 to 1150 mV versus Ag/AgCl. The as-prepared Pt–Bi/C sample shows the hydrogen adsorption/desorption region, which is almost diminished, whereas upon heat treatment shows hydrogen adsorption/desorption features. The peaks I and II observed during the forward scan corresponds to bismuth oxidation and the peak III on potential scan reversal corresponds to bismuth reduction in addition to the platinum reduction. The peak at ∼993 mV corresponds to bismuth oxidation to higher oxidation states [34]. The forward oxidation peaks I and II correspond to the stepwise oxidation of bismuth at the surface [43, 44].

A strong peak observed at ∼43 mV in the forward scan corresponds to bismuth stripping, which is absent upon heat treatment of Pt–Bi/C. Thus the heat treatment leads to the homogenization of Pt and Bi nanoparticles, whereas in the case of as-prepared sample it exists as simple solid solution form, as supported by XRD data. In the case of as-prepared Pt–Bi/C, bismuth atoms on the film are oxidized to bismuth oxide species and on cycle reversal they are stripped off the surface. Whereas, in the case of the heat treated ones, bismuth atoms entrapped in the platinum crystal lattice are not amenable to oxidation-driven stripping. Further, the Pt reduction current observed in the case of the heat treated sample is found to be smaller compared to that of the heat-treated sample, reflecting the fact that surface area decreases due to particle agglomeration.

It is also noted that repeated cycling to high positive potentials in sulphuric acid change the resulting CVs. The redox peaks at 703 and 43 mV ascribed to surface oxide formation and stripping, respectively grow with continuous cycling. This effect leads to surface roughening, as Bi is preferentially dissolved at high potentials. It is expected that Bi metal, being relatively unstable at positive potentials and in acidic media, tends to be in an ionic/oxidized form.

Figure 3 shows the cyclic voltammogram of Pt–Bi/C in 0.1 M $HClO_4$ at 100 mV s^{-1} in the potential range of −200 to 1150 mV versus Ag/AgCl. The peak observed at 674 and 645 mV versus Ag/AgCl for the heat treated and as-prepared samples, respectively, corresponds to platinum oxidation. The peak at 429 mV versus Ag/AgCl in the reverse scan, corresponds to platinum reduction and bismuth reduction from higher oxidation state to Bi metallic state, both occurring at very close potentials. Two reduction peaks were observed during the reverse scan of the heat treated Pt–Bi/C and the one at ∼553 mV corresponds to the platinum reduction and the other at ∼303 mV corresponds to the bismuth reduction. A bismuth stripping peak at ∼3 mV was also observed. Improvement in the hydrogen adsorption/desorption current is also observed for heat treated samples.

The cyclic voltammograms recorded in both sulphuric and perchloric acid for the as-prepared and heat-treated Pt–Bi/C in the potential range of −200 to 1150 mV versus Ag/AgCl exhibited, in general, a stripping peak at −17 mV corresponding to the reduction of the bismuth species leaching from the catalyst surface. However, this peak disappears immediately after the first cycle and does not show up during subsequent cycles and the response stabilizes, indicating that the catalyst surface is stabilized against any dissolution of the alloy constituents. Though this kind of behaviour has been mentioned by Abruna et al. [45], corresponding CV responses do not show the above mentioned features. The presence of the bismuth stripping peak indicates that partial dissolution of bismuth is part of the mechanism of surface oxidation of Pt–Bi. It is expected that a certain amount of residual bismuth species is always present on the catalyst surface (remaining un-reduced in the preparation stage) that undergo reduction during cyclic voltammetric examination.

3.3 Methanol oxidation reaction on nanoparticulate Pt–Bi/C

Figure 4 shows the cyclic voltammetric curves obtained for methanol oxidation in deoxygenated solutions of 0.5 M H_2SO_4 + 0.5 M CH_3OH. The voltammetric features are consistent with the literature reports and are typical of the electrooxidation of methanol on a platinum surface. In contrast to the Pt/C response, in the case of the Pt–Bi/C system the methanol activity is reduced and thus is resistant to methanol at a concentration of 0.5 M in the same potential interval explored. The small methanol oxidation wave observed in sulphuric acid on heat treated Pt–Bi/C constitutes 20% of the current observed for Pt/C, whereas on the as-prepared Pt–Bi/C it is barely 2% of the total methanol oxidation current recorded on Pt/C. In contrast, both as-prepared and heat-treated forms of Pt–Bi/C in perchloric acid do not show a methanol oxidation current and therefore the platinum bimetallic is remarkably resistant to the methanol oxidation reaction (MOR) in perchloric acid medium.

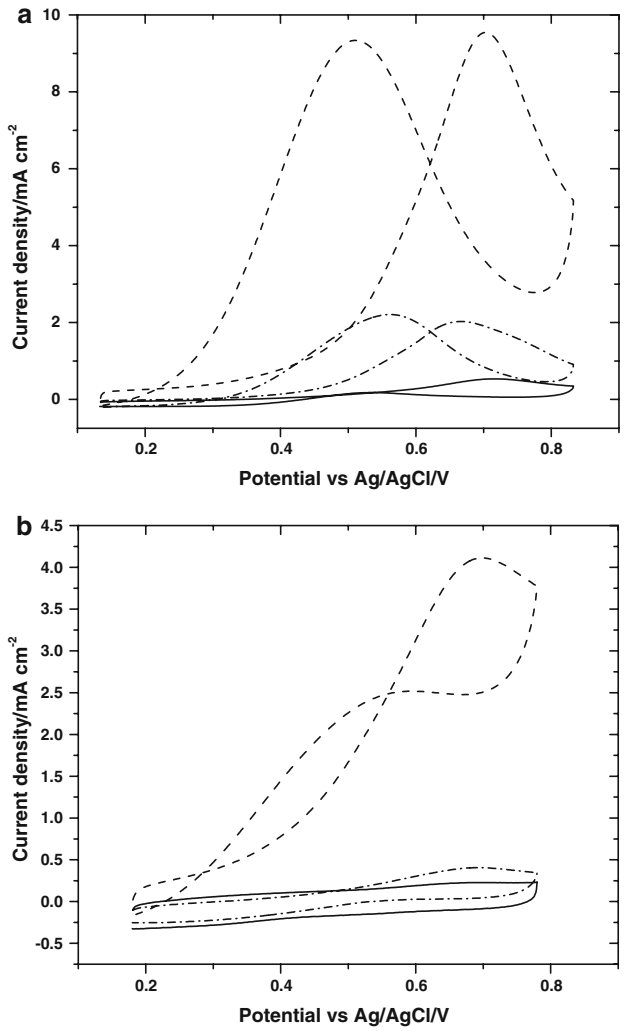

Fig. 4 Cyclic voltammograms of methanol oxidation on as-prepared (*solid line*), heat-treated (*dash-dotted line*) Pt–Bi/C and Pt/C catalysts (dashed line) in (**a**) 0.5 M sulphuric and (**b**) 0.1 M perchloric acid containing 0.5 M methanol with the scan rate of 100 mV s^{-1}

It can now be seen that while the Pt/C shows behaviour is as expected, Pt–Bi/C shows a clear difference with respect to the acid employed. In perchloric acid solutions, a near-total blocking of methanol oxidation can be seen, whereas in sulphuric acid, the features of MOR still persist. It is understood from Abruna's work [46] that methanol oxidation is totally inhibited on Pt–Bi and it is presumed that they have used perchloric acid medium. This may be explained by invoking the effect of anions on methanol oxidation. For example, it has been reported that bisulphate adsorption promotes methanol oxidation on Pt [47]. It is reasonable to explain this observation in terms of the formation of a porous bismuth sulphate film [48] during the reaction of Bi with water in the anodic potential excursions. As the reactions proceeds only with forced reduction, bismuth in these films can be reduced to Bi. In perchloric acid medium such porous films do not form and the only reaction possible is Bi dissolution and re-deposition [32]. It is now suggested that during the potential cycling, bismuth dissolves to a major extent and the Pt surface undergoes roughening. During this process, redistribution of Pt crystallites takes place, followed by Bi adsorption on these crystallites.

3.4 Stability of nanoparticulate Pt–Bi/C in acidic electrolytes

The surface stability of the Pt–Bi/C catalysts was examined by cycling the surface in the respective acid electrolyte and subsequently its activity towards methanol oxidation. This experiment involves, subjecting the catalyst surface to potential cycling in the range −200 to 1150 mV versus Ag/AgCl and transferring the treated-catalyst surface to a solution containing methanol. Figure 5 shows the methanol activity of the Pt–Bi/C surface at different levels of cycling in sulphuric and perchloric acid electrolytes and for comparison the performance of Pt/C in sulphuric acid is also presented in the figure. As can be observed from the cyclic voltammetric behaviour, the current due to methanol oxidation increases with increasing cycle number. The catalyst gradually becomes active for MOR. Obviously, bismuth leaching out from the surface in sulphuric acid is the cause of this effect. The heat-treated sample also initially shows an increase in MOR activity to gradually decrease with increasing cycle number. A plausible explanation is the surface enrichment by Pt, a situation similar to the formation of "Pt skin" on the catalyst particle [49]. Once the surface is enriched with Pt, due to its susceptibility to CO adsorption the activity again decreases. In perchloric acid medium, the cycling treatment does not affect the catalyst

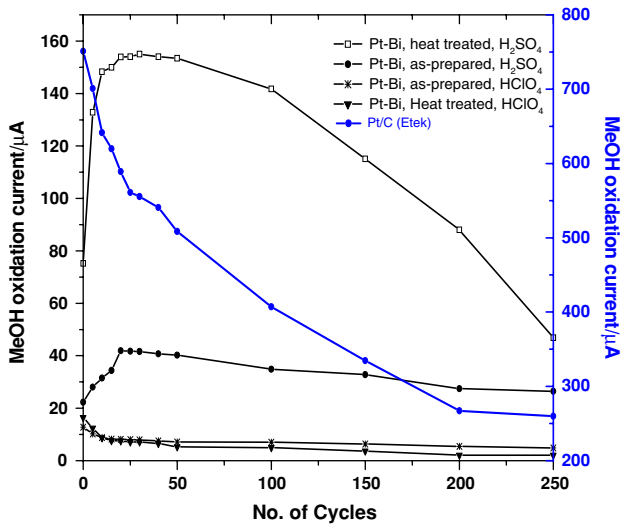

Fig. 5 Voltammetric stability of the Pt–Bi/C catalyst in terms of methanol oxidation current versus potential cycling treatment in perchloric and sulphuric acid electrolyte

surface and it retains methanol tolerance even up to 250 cycles with stable performance. It can now be stated that Pt–Bi/C (as-prepared or heat-treated) are unaffected by potential cycling and maintain methanol tolerance in perchloric acid solutions whereas they are active towards MOR in sulfuric acid solutions. This behaviour highlights the importance of anion effects on the Pt–Bi/C catalyst stability.

3.5 RDE and RRDE oxygen reduction reaction at nanoparticulate Pt–Bi/C

In order to understand the kinetics of ORR in the presence and absence of methanol RRDE experiments were carried out with the Pt–Bi/C catalyst materials. In these studies, the potential was swept at 5 mV s^{-1} from 900 to −100 mV versus Ag/AgCl (potential region of ORR) in sulphuric and perchloric acid electrolytes.

Figure 6a shows the hydrodynamic polarization curves of as-prepared and heat treated Pt–Bi/C in oxygen-saturated solutions of 0.5 M sulphuric acid with and without 0.5 M methanol at a rotation rate of 1,600 rpm. The ORR half wave potential and the current densities calculated by normalizing to the geometric electrode area are given in Table 1. The half-wave potential of ORR polarization is shifted anodically by 40 mV with respect to that of the as-prepared sample and a slight increase in the limiting current density is observed after heat treatment. Addition of methanol causes a cathodic shift of the half-wave potential by approximately 100 mV in both cases. Moreover, the MOR-activity of the catalyst is conspicuous by the presence of a current peak at ∼600 mV, typical of methanol

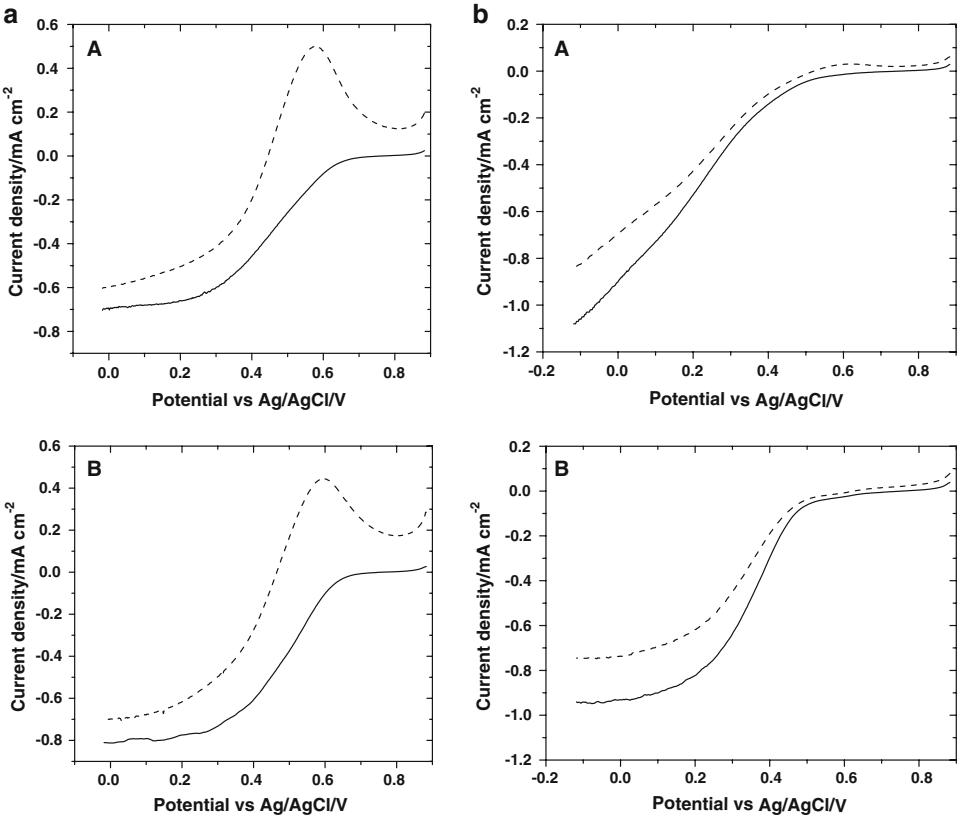

Fig. 6 (**a**) Linear sweep voltammograms of ORR of (A) as-prepared and (B) heat-treated Pt–Bi/C with (*dotted line*) & without (*solid line*) 0.5 M methanol in 0.5 M sulphuric acid; scan rate: 5 mV s^{-1}; $\omega = 1{,}600$ rpm. (**b**) Linear sweep voltammograms of ORR of (A) as-prepared and (B) heat-treated Pt–Bi/C with (*dotted line*) and without 0.5 M methanol (*solid line*) in 0.1 M perchloric acid; scan rate: 5 mV s^{-1}; $\omega = 1{,}600$ rpm

Table 1 Parameters derived from hydrodynamic polarization curves

System	Electrolyte	Onset potential, /mV at 1,600 rpm	ORR current density, /mA cm^{-2}	No. of electrons for ORR	Tafel slope /mV dec^{-1}	H_2O_2 calculated (%)
As-prepared Pt–Bi/C	0.5 M H_2SO_4	628	0.71	3.56	75/175	0.38
	0.5 M H_2SO_4 + 0.5 M MeOH	563	0.62	3.74	>400	0.47
	0.1 M $HClO_4$	393	0.88	3.99	~400	0.27
	0.1 M $HClO_4$ + 0.5 M MeOH	403	0.70	4.01	~400	0.18
Heat-treated Pt–Bi/C	0.5 M H_2SO_4	633	0.81	3.69	90/150	0.39
	0.5 M H_2SO_4 + 0.5 M MeOH	548	0.70	3.64	>400	0.33
	0.1 M $HClO_4$	463	0.96	3.71	120	0.22
	0.1 M $HClO_4$ + 0.5 M MeOH	458	0.75	3.58	135	0.13

oxidation even though the Pt–Bi/C subjected to heat treatment, due to the leaching/selective dissolution of bismuth into the sulphuric acid electrolyte results in the formation of "*Pt skin*"' that favours MOR. This behaviour may be contrasted with the observations made when perchloric acid is employed as electrolyte. The polarization curve in Fig. 6b shows that the ORR current does not reach steady-state in the case of the as-prepared catalyst and the polarization curves are ill-defined. This is presumably due to the dissolution of one of the constituents of the catalyst. In perchloric acid solutions, the heat-treated catalyst presents well-defined polarization behaviour and in both cases, methanol does not seem to undergo oxidation as evidenced by the absence of the corresponding current peak. However, there is a cathodic shift of ~40 mV in the half-wave potential value. This is also associated with a 22% fall in the current density value in the presence of methanol. Thus, in spite of the observation that the catalyst is "silent" towards the oxidation of methanol, the presence of the latter affects the ORR current. It is now appropriate to bring in the cases of Pt bimetallics where this type of non-ideal methanol-tolerant behaviour was observed. It appears that a "trade off" is common with all the known so called methanol tolerant combinations of Pt [18, 30, 50].

The voltammograms for ring and disk in a RRDE setup at different rotation rates for the Pt–Bi/C modified GC electrode (both as-prepared and heat treated) in oxygen-saturated acid solutions at 25 °C were performed. The potential regions under kinetic and oxygen mass transport limiting control are clearly observed for all the rotation rates and the current density increases with rotation rate as the mass transport of molecular oxygen to the electrode surface becomes facile. For quasi-steady state conditions and assuming all of the reactions to be first order with respect to the oxygen concentration, the observed current, i, for a mixed kinetic-diffusion controlled reaction depends on the rotation rate according to the Koutecky–Levich equation [51].

$$\frac{1}{i}=\frac{1}{i_k}+\frac{1}{i_d}=\frac{1}{i_k}+\frac{1}{0.2nFD_o^{2/3}\omega^{1/2}\nu^{-1/6}C_o}=\frac{1}{i_k}+\frac{1}{B\omega^{1/2}} \quad (1)$$

where i_k is the kinetic current, B is the Levich slope, 'n' the number of electrons involved in the ORR per oxygen molecule, 'C' the saturation concentration for oxygen in the electrolyte (1.26×10^{-3} M), 'D' is the diffusion coefficient (1.93×10^{-5} cm^2 s^{-1}), 'ν' the kinematic viscosity of the solution (1.009×10^{-2} cm^2 s^{-1}) and 'ω' is the rotation rate in rpm.

The number of electrons involved in the ORR was calculated using the Koutecky–Levich equation, which relates the current i to the rotation rate of the electrode ω. The Koutecky–Levich plot, $1/i$ versus $1/\omega^{1/2}$, for Pt–Bi/C under mass transport control at an electrode potential ~3 mV was plotted (Figures not shown) and using the slope of the resulting linear relationship, the value for n was calculated (Table 1), which is consistent with previous results for Pt based catalyst materials using a rotating ring-disk electrode [25, 52]. This suggests that the ORR on Pt–Bi/C proceeds via the direct pathway involving the dual-site adsorbed oxygen species.

$$Pt + O_2 \rightarrow Pt - O_{2(ads)} \underset{2e^-}{\overset{2H^+}{\rightarrow}} Pt(OH)_2 \underset{2e^-}{\overset{2H^+}{\rightarrow}} Pt + 2H_2O \quad (2)$$

since even at highly active surfaces, like Pt and its alloys, the ORR proceeds at least partially via the peroxide route having n values slightly less than 4. This was further verified by calculating the % of H_2O_2 produced during the ORR from the ring current using the equation:

$$\%\ H_2O_2 = \frac{2I_R/N}{I_D + (I_R/N)} \quad (3)$$

where I_D and I_R are the disk and ring currents, respectively and N is the collection efficiency of the RRDE. The ring currents are obtained from the controlled rotating ring disk electrochemical studies employing Pt ring and disk electrodes rotating at 1,600 rpm, where the ring electrode was kept at 1.073 V in order to oxidize any H_2O_2 released

during O_2 reduction at the disk electrode; H_2O is not oxidized at this potential. The collection efficiency of the ring disk was measured to be $N = 0.24$ (that is, 24% of the products released by the disk were detected at the ring) and the % of H_2O_2 generated are given in Table 1. The peroxide percentage observed is a negligible quantity and this result strongly suggests a high electrochemical efficiency of the Pt–Bi electrocatalyst, where virtually all of the O_2 is directly reduced to H_2O.

The kinetic current i_k can be obtained by extrapolation of the Koutecky–Levich plots for $\omega^{-1/2} \rightarrow 0$. From the kinetic current, the Tafel slopes were calculated by plotting log i_k versus potential (Figures not shown) and are given in Table 1. The Tafel slope values calculated are 75 and 90 mV dec^{-1}, indicating a chemical step following a fast first electron transfer is the rate-determining step. As is commonly observed for ORR, the Tafel plots exhibit two distinct slopes at low (>550 mV) and high (<500 mV) overpotentials. Similar slope values for Pt based catalysts are reported in the literature within these two potential regions [52–54], suggesting that the ORR mechanism remains the same. However, the shape of the Tafel plot is slightly different with a single Tafel slope value of 120 mV dec^{-1}, suggesting that breaking of O–O bond is the slow step for the heat treated sample of Pt–Bi/C examined in perchloric acid [55]. For the systems with Tafel slope above 400 mV dec^{-1}, the reaction mechanism is affected by the adsorption of methanol molecules or the presence of bisulphate ion, which greatly affect the ORR mechanism.

The results obtained in these studies indicate that the Pt–Bi/C catalyst material has properties and reactivity that are dramatically different from those of surfaces in perchloric and sulphuric acid with respect to oxygen reduction and methanol tolerant activity. However, the onset potential of ORR is significantly shifted negatively by over 100 mV and, at the same time, the current density is significantly enhanced. In general, the Pt–Bi surface appears to have a dramatically lower sensitivity towards methanol activity compared to pure platinum.

In sulphuric acid, above 500 mV or at a positive potential, bismuth selectively leaches out from the electrode surface leaving a '*Pt skin*'. Daniele et al. [34] reported that the upper potential limit above 550 mV versus Ag/AgCl led to partial bismuth dissolution (selective dissolution/leaching) with a concomitant increase of the hydrogen adsorption/desorption peaks. Bismuth, once in the acidic electrolyte as its oxide form, immediately converts to its sulphate form and does not re-deposit on the electrode surface readily. Thus the formation of the "*Pt skin*" on the electrode surface leads to methanol activity, which also affects the kinetics of ORR.

The higher ORR current in sulphuric acid medium is attributed to the adsorption of the bisulphate ion (HSO_4^-), a tetrahedral anion which adsorbs strongly on Pt(111) [56] which results in inhibitory effects of PtOH, a factor favourable for ORR.

In perchloric acid, bismuth dissolves from the electrode surface during cycling and may interact with the perchlorate anion. During the reverse scan bismuth is deposited or enters the Pt crystal lattice. Hence the Pt–Bi alloy structure is not affected by the electrochemical process and the alloy structure is retained which, in turn, helps maintaining methanol tolerance of the catalyst surface. We are presently investigating the beneficial role of bismuth on the performance of single cells and this will be reported separately.

4 Conclusions

Carbon-supported Pt–Bi nanoparticle catalysts were prepared using a polyol method and characterized for particle size, crystal structure and extent of alloy formation. The electrochemical studies of the as-prepared and heat-treated catalysts in perchloric and sulfuric acid electrolytes showed that bismuth dissolution (oxidative cycle) and re-deposition (reductive cycle) to be a common feature, to different extents. The catalyst stability under potential cycling conditions is observed to be much higher in perchloric acid than sulfuric acid. While there is total absence of methanol oxidation reaction on these catalysts when examined in perchloric acid, the same in sulfuric acid medium exhibits methanol oxidation characteristics, though to a limited extent. The oxygen reduction reaction, studied using RDE and RRDE voltammetry is found to involve four-electron pathway irrespective of the presence of methanol, as also noted from the Tafel analysis. The onset potential for ORR is shifted by about 100 mV to more negative values and at the same time the current density is significantly enhanced. This type of non-ideal methanol-tolerant behaviour among Pt bimetallics and a "trade off" is common with all the known so-called methanol tolerant combinations of Pt. In general, the as-prepared Pt–Bi shows a balance of ORR activity and methanol tolerance in perchloric acid. Hence, it is now suggested that before attempting DMFC fabrication, it is preferable to test the performance of the catalysts in electrolytes containing perchloric acid rather than sulfuric acid medium.

Acknowledgments The authors thank the Department of Science & Technology, New Delhi for financial assistance [SR/S1/PC-37/2004] and Professor A. K. Shukla, Director, CECRI for his encouragement.

References

1. Arico AS, Srinivasan S, Antonucci V (2001) Fuel Cells 1:133
2. Baranton S, Coutanceau C, Roux C, Hahn F, Leger J-M (2005) J Electroanal Chem 577:223

3. Lu Y, Reddy RG (2007) Electrochim Acta 52:2562
4. Chu D, Jiang R (2002) Solid State Ionics 148:591
5. Wang X, Waje M, Yan Y (2004) J Electrochem Soc 151:A2183
6. Reeve RW, Christensen PA, Hamnett A, Haydock SA, Roy SC (1998) J Electrochem Soc 145:3463
7. Schmidt TJ, Paulus UA, Gasteiger HA, Vante NA, Behm RJ (2000) J Electrochem Soc 147:2620
8. Ozenler SS, Kadirgan FJ (2006) J Power Sources 154:364
9. Papageorgopoulos DC, Liu F, Conrad O (2007) Electrochim Acta 53:1037
10. Raghuveer V, Ferreira PJ, Manthiram A (2006) Electrochem Commun 8:807
11. Fernandez JL, Raghuveer V, Manthiram A, Bard AJ (2006) J Am Chem Soc 127:13100
12. Low Pt Loading Fuel Cell Electrocatalysts, DOE Hydrogen Program FY (2005) Progress report pp 828–832
13. Wang W, Zheng D, Du C, Zou Z, Zhang X, Xia B, Yang H, Akins DL (2007) J Power Sources 167:243
14. Zhang L, Lee K, Zhang J (2007) Electrochim Acta 52:3088
15. Mustain WE, Kepler K, Prakash J (2006) Electrochem Commun 8:406
16. Tarasevich MR, Chalykh AE, Bogdanovskaya VA, Kuznetsova LN, Kapustina NA, Efremov BN, Ehrenburg MR, Reznikova LA (2006) Electrochim Acta 51:4455
17. Shao MH, Huang T, Liu P, Zhang J, Sasaki K, Vukmirovic MB, Adzic RR (2006) Langmuir 22:10409
18. Shukla AK, Raman RK, Choudhury NA, Priolkar KR, Sarode PR, Emura S, Kumashiro R (2004) J Electroanal Chem 563:181
19. Yuan W, Scott K, Cheng H (2006) J Power Sources 163:323
20. Paffett MT, Beery JG, Gottesfeld S (1988) J Electrochem Soc 135:1431
21. Salgado JRC, Antolini E, Gonzalez ER (2005) Appl Catal B Environ 57:283
22. Beard BC, Ross PN (1990) J Electrochem Soc 137:3368
23. Toda T, Igarashi H, Watanabe M (1999) J Electroanal Chem 460:258
24. Neergat N, Shukla AK, Gandhi KS (2001) J Appl Electrochem 31:373
25. Koffi RC, Coutanceau C, Garnier E, Leger J-M, Lamy C (2005) Electrochim Acta 50:4117
26. Yang H, Coutanceau C, Leger J-M, Vante NA, Lamy C (2005) J Electroanal Chem 576:305
27. Beck NK, Steiger B, Scherer GG, Wokaun A (2006) Fuel cells 6:26
28. Xia D, Chen G, Wang Z, Zhang J, Hui S, Ghosh D, Wang H (2006) Chem Mater 18:5746
29. Roychowdhury C, Matsumoto F, Zeldovich VB, Warren SC, Mutolo PF, Ballesteros M, Wiesner U, Abruna HD, DiSalvo FJ (2006) Chem Mater 18:3365
30. Yang H, Vante NA, Leger J-M, Lamy C (2004) J Phys Chem B 108:1938
31. Campbell SA, Parsons R (1992) J Chem Soc Faraday Trans 88:833
32. Schmidt TJ, Stamenkovic VR, Lucas CA, Markovic NM, Ross PN Jr (2001) Phys Chem Chem Phys 3:3879
33. Roychowdhury C, Matsumoto F, Mutolo PF, Abruna HD, DiSalvo FJ (2005) Chem Mater 17:5871
34. Daniele S, Bergamin S (2007) Electrochem Commun 9:1388
35. Casado-Rivera E, Gal Z, Angelo ACD, Lind C, DiSalvo FJ, Abruna HD (2003) Chem Phys Chem 4:193
36. Schmidt TJ, Behm RJ, Grgur BN, Markovic NM, Ross PN Jr (2000) Langmuir 16:8159
37. Smith SPE, Ben-Dor KF, Abruna HD (1999) Langmuir 15:7325
38. www.abruna.chem.cornell.edu/chem629/lectures/lecture24.pdf
39. Do J-S, Chen Y-T, Lee M-H (2007) J Power Sources 172:623
40. Remona AM, Phani KLN (2007) Chem Mater 19:1529
41. Xia D, Chen G, Wang Z, Zhang J, Hui S, Ghosh D, Wang H (2007) Chem Mater 19:1530
42. Silvert PY, Vijayakrishnan V, Vibert P, Herrera-Urbina R, Elhsissen KT (1996) Nanostruc Mater 7:611
43. Lee J, Strasser P, Eiswirth M, Ertl G (2001) Electrochim Acta 47:501
44. Uhm S, Yun Y, Tak Y, Lee J (2005) Electrochem Commun 7:1375
45. Volpe D, Casado-Rivera E, Alden L, Lind C, Hagerdon K, Downie C, Korzeniewski C, DiSalvo FJ, Abruna HD (2004) J Electrochem Soc 151:A971
46. Casado-Rivera E, Volpe DJ, Alden L, Lind C, Downie C, Vázquez-Alvarez T, Angelo ACD, DiSalvo FJ, Abruna HD (2004) J Am Chem Soc 126:4043
47. Jarvi TD, Stuve EM (1998) In Lipkowski J, Ross PN (eds) Electrocatalysis. Wiley-VCH, p 112
48. Li WS, Long XM, Yan JH, Nan JM, Chen HY, Wu YM (2006) J Power Sources 158:1096
49. Stamenkovic V, Schmidt TJ, Ross PN, Markovic NM (2002) J Phys Chem B 106:11970
50. Mathiyarasu J, Phani KLN (2007) J Electrochem Soc 154:B11005
51. Bard AJ, Faulkner LR (2001) Electrochemical methods, 2nd edn. John Wiley & Sons, Inc, NY
52. Ye H, Crooks RM (2007) J Am Chem Soc 129:3627
53. Demarconnay L, Coutanceau C, Leger J-M (2008) Electrochim Acta 53:3232
54. Paulus UA, Wokaun A, Scherer GG, Schmidt TJ, Stamenkovic V, Markovic NM, Ross PN (2002) Electrochimica Acta 47:3787
55. Adzic R (1998) In Lipkowski J, Ross PN (eds) Electrocatalysis. Wiley-VCH, p 210
56. Faguy PW, Marinkovic NS, Adzic RR (1996) Langmuir 12:243